Received: 2 May 2024 | Revised: 3 July 2024 | Accepted: 10 July 2024

DOI: 10.1002/pc.28826

RESEARCH ARTICLE

spe INSPIRING PLASTICS PROFESSIONALS Polymer COMPOSITES WILEY

Experimental and statistical damage analysis in milling of S2-glass fiber/epoxy and basalt fiber/epoxy composites

Ahmed Cagri Sayin[1] | **Sengul Danisman**[2] | **Emin Ersoy**[2] | **Cagatay Yilmaz**[1] | **Sinan Kesriklioglu**[1]

[1]Department of Mechanical Engineering, Abdullah Gul University, Kayseri, Turkey

[2]Department of Mechanical Engineering, Erciyes University, Kayseri, Turkey

Correspondence
Sinan Kesriklioglu, Department of Mechanical Engineering, Abdullah Gul University, Kayseri, Turkey.
Email: sinan.kesriklioglu@agu.edu.tr

Funding information
Scientific and Technological Research Council of Türkiye, Grant/Award Number: TUBITAK 1001-221M085

Abstract

S2-glass fiber reinforced plastics (S2-GFRP) and basalt fiber reinforced plastics (BFRP) have emerged as crucial materials due to their exceptional mechanical properties, and milling of composite materials plays an important role in achieving desired properties. However, they have proven challenges due to relative inhomogeneity compared with metals, resulting unpredictability in quality of milling operations. The objective of this work is to investigate the effect of cutting parameters, tool geometry and tool surface materials on the surface quality of composites using burrs as a metric. S2-GFRP and BFRP composites were produced by the vacuum infusion method. Helical and straight flute end mills were manufactured from high-speed steel (HSS) and carbide rounds, and half of them were coated with titanium nitride using reactive magnetron sputtering technique. Taguchi L18 orthogonal array is used to determine the effect of tool material, tool angle, coating, cutting direction, spindle speed, and feed rate on the machining quality of S2-GFRPs and BFRPs with respect to burr formations. Milling experiments were conducted under dry conditions and then the burrs were imaged to calculate the total area and length. Statistical analysis was also performed to optimize the machining parameters and tool type for ensuring the structural integrity and performance of the final composite parts. The results showed that the selection of tool material has the most significant impact on the burr area and length of the machined surface. The novel image analysis allows to analyze the extent of the burr size with a desirable operation speed for industrial applications.

Highlights

- Aerospace grade S2-Glass (S2-GFRP) and basalt fiber reinforced plastics (BFRP) were manufactured.
- Carbide and HSS end mills were fabricated and coated with titanium nitride protective layer.
- FRPs were machined at various process parameters designed by Taguchi method.
- Distinctive image processing was firstly used to compute milling induced Burr area and length.

- Statistical analysis was performed to quantify the contribution of parameters and optimize milling.

KEYWORDS

basalt, coating, composite, image analysis, precision milling, S2-glass, sustainable manufacturing

1 | INTRODUCTION

Fiber reinforced polymers (FRPs) along with thermoset polymers are emerging materials for achieving high mechanical and structural properties, high strength-to-weight ratio, low specific gravity, versatility, and controllable anisotropy, and thermoset polymers such as epoxy resin are receiving considerable attention as a matrix for FRP in the recent composite literature.[1,2] Glass fiber reinforced plastics (GFRP) are one of the most important types of FRP and expected to have the largest volume and value in the composite market by 2025.[3] Among the glass fiber reinforced plastics, S2-glass reinforced plastic (S2-GFRP) is renowned for its exceptional tensile strength, low density, high gamma radiation resistance, and high chemical stability and impact strength.[4,5] On the other hand, basalt fiber reinforced plastics (BFRP) find utility in fire-resistant textiles, reinforced concrete structures, and ballistic protection applications with their exceptional resistance to heat, mechanical robustness, high failure strain and corrosion resilience. Both composite materials have applications in the aerospace, automotive, and aeronautical sectors.[3,6,7] Researches on fibers suggested that basalt fibers have similar mechanical properties with glass fibers, with continuous basalt fibers possessing comparable strength to glass fibers,[8,9] yet their machinability can vary significantly due to the different structures and compositions of the fibers.

Milling of S2-GFRP and BFRP is an important process that impacts the final properties and performance of these materials. Main purpose of milling process for fiber reinforced plastic is to shape and surface finish.[10] The cases where composite parts are manufactured near-net shape, often requiring postprocessing to remove excess material. Milling is used to fine-tune the final product due to its high precision.[11] Optimization of milling process in a cost-effective fashion allows to improve availability of the composites.[12]

Machining of composite materials often results with formation of delamination. Detection of the delamination is important since the damage to the composites is accumulated rather than an instant failure in case the initial damage criteria have exceeded.[13,14] Colligan and Ramulu[15] documented three types of delamination modes: Type I delamination refers to damage in a form of tear on the surface with uncut fibers, Type II delamination, also referred as "burr" suggests an uncut fiber with no damage done to the base material, and Type III delamination suggests "fuzzy" attachment of fibers to machined surface.[15,16] In literature, Type I delamination is widely discussed since it has a direct effect on the fatigue life of the composite, can directly lead to through-the-thickness failure, reducing the material's overall strength due to the internal damage to fibers and/or composite structure, and causes sub-optimal assembly tolerance.[17–20] Drilling-induced Type I delamination is reported to result 60% of all part rejection in aircraft industry.[21] Research on Type II delamination is notably less extensive than that on Type I. It is possible to remove Type II delamination, along with the excess section of Type I delamination with edge trimming or grinding to ensure surface finish for high-precision applications. However, it brings another set of challenges, increasing the probability of permanent damage on the composite.[22,23]

Due to their heterogeneity, GFRP composites present a set of complicated challenges.[24] The understanding of geometrical (i.e., rake angle and helix angle) and cutting parameters (i.e., cutting speed and feed rate) is crucial for optimizing the machining process of the composite materials.[25] Evidently, the effectiveness of milling is dependent on the surface quality, tool life, cutting forces, and temperatures.[16,26] Glass fiber-reinforced composites have been investigated for the machinability of these materials to understand the milling performance and its effects on surface finish and tool wear.[27] Machining parameters such as cutting speed, feed rate, metal removal depth, and cutting tool surface properties are important factors affecting tool performance in the machining of composites. Sarma et al.[17] investigated the effect of cutting speed and cutting depth to cutting strength in GFRP tubes with cubic boron nitride tools using a lathe. The research group experimented the combinations of feed rate of 0.048, 0.096, 0.143 0.191, and 0.238 mm/rev with spindle speed of 54, 82, 126, 194, and 302 m/min, and concluded that low feed rate and high cutting speed. Hocheng et al.[18] examined the effects of tool geometry high-speed steel (HSS) drill bits of 10 mm diameter to delamination

of carbon fiber reinforced composites. Among twist, saw, candle stick, core and step drills, research group suggested that step drill is suitable for highest feed rate operations with minimal delamination. Jenarthanan et al.[19] suggested a mathematical model for milling induced damage analysis in GFRPs. Among the combinations of cutting speed of 50, 100, and 150 m/min and feed rate of 0.10, 0.15, and 0.20, the group concluded that feed rate significantly increases delamination factor while cutting speed has little effect on it. Kilickap[20] studied drilling parameters on GFRP with cutting speed of 10, 15, and 20 m/min with feed rate of 0.1, 0.2, and 0.3 mm/rev using a 5 mm cemented carbide tool. The researcher suggested that delamination around the hole increases with both cutting speed and feed rate.

Ekici et al.[28] proposed an image processing approach for calculating the area of uncut fibers around the drilled holes for carbon-fiber/aluminum composites. The researchers used a multi-mapped image processing model (MMIPM) in MATLAB in order to profile the uncut fibers. The researchers aimed to enhance the precision of the hole drilling process. Venkateshwaran and Elaayaperumal[29] utilized an image analysis method of C-scan on banana fiber/epoxy composites, which utilizes the sound waves to visualize the damage during the machining. The researchers have used the spindle speed values of 500, 1000, 1500, and 2000 mm/min and feed rate values of 0.1, 0.2, and 0.3 mm/rev, and concluded that increased spindle speed and feed rate resulted in increased delamination factor. Hrechuk et al.[30] introduced an image analysis algorithm in order to measure the uncut fibers in drilled holes and rank them according to the area of uncut fibers. Their research contributes to the improvement of hole quality of composites by investigating the uncut fibers from carbon fiber-reinforced polymers (CFRP).

Milling direction is also another important parameter and significantly influences the machining quality of the composite parts. Conventional milling involves the rotation of the tool in a direction opposing the feed motion, resulting in intermittent cutting, and increasing the surface roughness. Research suggests that conventional milling with a 6 mm 4 flutes carbide tool, results with greater surface roughness on horizontal milling compared with climb milling, while climb milling has shown better results for inclined surfaces on carbon fiber reinforced composites.[26] On the other hand, climb milling, characterized by the rotation of the tool in the same direction as the feed motion, can sometimes lead to more vibration on the workpiece and material deformation.[31]

Rao et al.[32] suggested that for the milling process position of fiber failure in the form of chips can be predicted in unidirectional-fiber reinforced polymers using finite element analysis. Azmi et al.[33] discussed the effects of feed rate and cutting speed during machining to tool life of uncoated cemented carbide tools. The research group concluded that cutting speed is the dominant factor of tool life, also suggested that the uncut fibers affected the tool wear significantly. Yardimeden[34] analyzed the effect of cutting speed feed rate and tool radius of cemented carbide tools to surface roughness on E-glass FRP. The author confirmed that high cutting speed and low feed rate results with optimum surface finish, and increased tool radius decreases surface roughness. Sait et al.[35] implemented the desirability analysis of Taguchi method with the parameters of flank and crater wear, machining force and surface roughness. Research group suggested that low feed rate and moderate cutting velocity resulted in the optimum machining parameters for hand layup GFRP while moderate feed rate and cutting velocity is optimum for filament wound GFRPs.

Surface coatings are one of the most effective ways to improve tool surface properties.[36–38] Knap et al.[39] suggested that thickness and type of coating, in their case UNICO and CrN coating, has significant effect on surface roughness during the milling of GFRP. Among the chemical vapor deposition (CVD) and physical vapor deposition (PVD) techniques used in this field, titanium-based coating types obtained by magnetically induced sputtering method stand out with their mechanical and tribological properties.[40–44] In composite machining, tools coated with the CVD method reveal higher cutting forces than tools coated with the PVD method, and PVD tools show better smooth cutting ability. Considering the abrasive effect of fibers and contact loads, tool quality and selection are very important.[45] Titanium-based coating types that increase tool performance serve the desired machining quality under machining conditions.[36,42,46,47] In the harsh machining conditions of composites, the tool material must combine high hardness and high toughness.[45] Therefore, TiN thin films are widely used with their advantages in machining.[43] Studies involving composite milling uses surface roughness as a parameter for surface quality, and research on burr formation predominantly focuses on drilling process. There is still a lack of research that involves optimization of burr formation with image analysis for milling operations.

This study undertakes the task of evaluating milling quality in both S2-GFRP and BFRP, employing a novel methodology centered around "burr," Type II and external sections of Type I delamination, using image analysis to compute the total area and maximum burr length for the first time in the literature for milling process. The aim of this academic endeavor is to determine the effect of machining parameters, such as spindle speed, feed rate, tool material, tool geometry, and tool coating on the burr area and burr length for milling operations in order to reduce the negative effects of uncut fibers. The presented burr analysis allows the quantification of the cumulative burr area and length resulting from the milling processes, serving as a quantitative measure for evaluating

machining quality. Additionally, it involves analyzing the burrs formed during the machining of these composites under dry cutting conditions using both uncoated and titanium nitride (TiN)-coated end mills, with a focus on optimizing machining parameters and types of the cutting tool. By increasing the available knowledge of S2-GFRP and BFRP materials in the literature, an increase in the usage of those materials in the industry is expected.

2 | MATERIALS AND METHODS

BFRP and S2-GFRP plates were produced using the vacuum infusion method. Helical and straight flute tungsten carbide and HSS end mills were manufactured, and three of the tools were coated with a protective layer. Cutting tests were then conducted under dry condition to study the effect of cutting geometry and surface condition on the machining quality of composite structures. Image analysis was also carried out using ImageJ software to quantify the damage area and optimize the milling process.

2.1 | Fabrication of and characterization composite plates

The vacuum infusion method was used to produce both S2-GFRP and BFRP. Within the recommended range for delamination observation, the thickness of the plate was set to be approximately 3.6 and 2.7 mm for BFRP and S2-GFRP, respectively. The fibers and consumable layers consisting of the peel ply, vacuum bag, release layer, and resin flow mesh layer, are cut into desired sizes. The entire system is put under a vacuum and covered by the vacuum bag. The previously prepared resin is sucked into the system from the opposite side of the vacuum. Prior to impregnation of fiber with resin, a leak test was performed by monitoring the manometer attached to bagged system for 10 min after the pump turned off the air intake. Once airtightness is achieved, the raw epoxy (Sika Biresin CR122) is mixed with the hardener (Sika Biresin CR122-5) in 100:30 weight ratios. To purify the mixture from air, it is placed in a closed container and the air is vacuumed with a vacuum pump. After the mixture is degassed for 10 min, it is placed in a container and the end of the pipe is placed in it. The aluminum plate of the infusion table is then heated to approximately 90°C and held at this level for 18 h for both fiber composites to achieve proper curing. After the system was cooled down to room temperature, the composite material was ready to be processed. The simple-weave fibers are stacked such that the weave pattern of each layer aligned perfectly with the layer below, ensuring precise registration and uniformity for the composite materials. Properties of fibers are shown in Table 1. Mechanical properties of the produced composite plates, such as Young's modulus and tensile strength are determined with a servo-hydraulic tension/compression/fatigue test machine (Instron 8801). Diameters of the S2-glass and basalt fibers were measured on the optical microscope (ZEISS Axio Imager 2). The material and mechanical properties of S2-GFRP and BFRP composite plates are listed in Table 1. Burn-out tests are conducted based on the ASTM D2584 standard to determine the fiber volume fraction according to:

$$V_f = \left[\frac{\rho_m * w_f}{\rho_m * w_f + \rho_f * w_m}\right], \quad (1)$$

where ρ_m and ρ_f are the density, w_m and w_f are weights of the matrix and fibers, respectively, in S2-GFRP and BFRP composite plates. Burn-out tests are repeated three times to ensure consistency. For basalt samples, the volume fraction values were 48%, 47%, and 46% while for S2-GFRP samples, it is 58%, 61%, and 58%. The average of the values is noted in Table 1.

2.2 | Manufacturing and coating of end mills

The experimental methodology revolves around three principal tools: The helical HSS tool, characterized by a 10 mm HSS DIN327 milling tool featuring a rake angle of 12° and a cutting angle of 25°, the straight carbide tool, a carbide tool with a cutting angle of 0° and the Helical carbide tool, machined to mimic the properties of the helical HSS tool, thereby retaining identical angular specifications. Detailed depictions of these tools can be seen in Figure 1. The

TABLE 1 Material and mechanical properties of S2-glass fiber reinforced plastics (S2-GFRP) and basalt fiber reinforced plastics (BFRP) composite plates.

Material	Young's modulus (GPa)	Tensile strength (MPa)	Fiber diameter (μm)	Layers of fibers	Fabric GSM	Weave type	Fiber volume fraction
BFRP	18.88	487	10	22	220	Plain	47%
S2-GFRP	19.87	588	11	4	800	Plain	59%

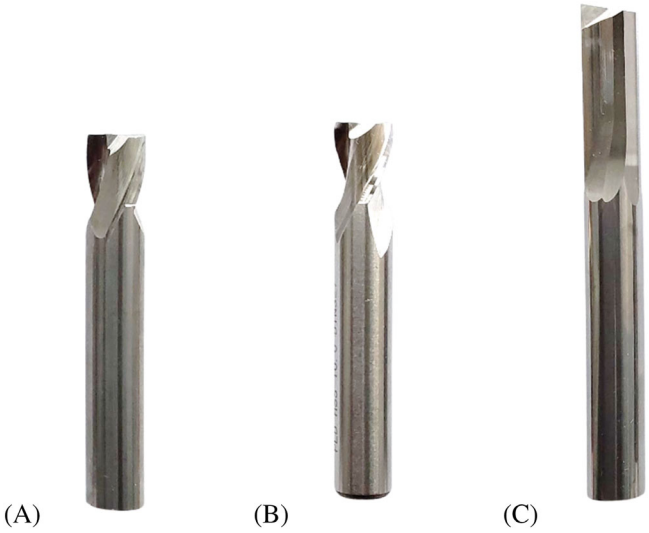

FIGURE 1 (A) Helical carbide, (B) helical high-speed steel, and (C) straight carbide tools used in the milling of composites.

helical HSS tool was bought from an external supplier. The end mills were geometrically characterized and fabricated in a CNC grinding machine. Raw materials for carbide tools were supplied from Boehlerit[48] and consist of 94 wt% tungsten carbide and 6 wt% cobalt with a Vicker's hardness of 1825 in HV30 standards.

TiN thin films were deposited onto the cutting tools used in milling operations by the reactive magnetron sputtering technique. The deposition and characterization processes of thin TiN films are illustrated schematically in Figure 2. Before the coating process, the cutting tools and the samples used in the analysis were cleaned in an ultrasonic bath containing acetone and alcohol for 5 min each. A 650 by 110 mm titanium target with a 99.99% purity was used in the coating process. TiN thin films were deposited using an asymmetric bipolar DC power supply. The nitrogen gas flow rate was automatically controlled via optical emission spectroscopy (OES)

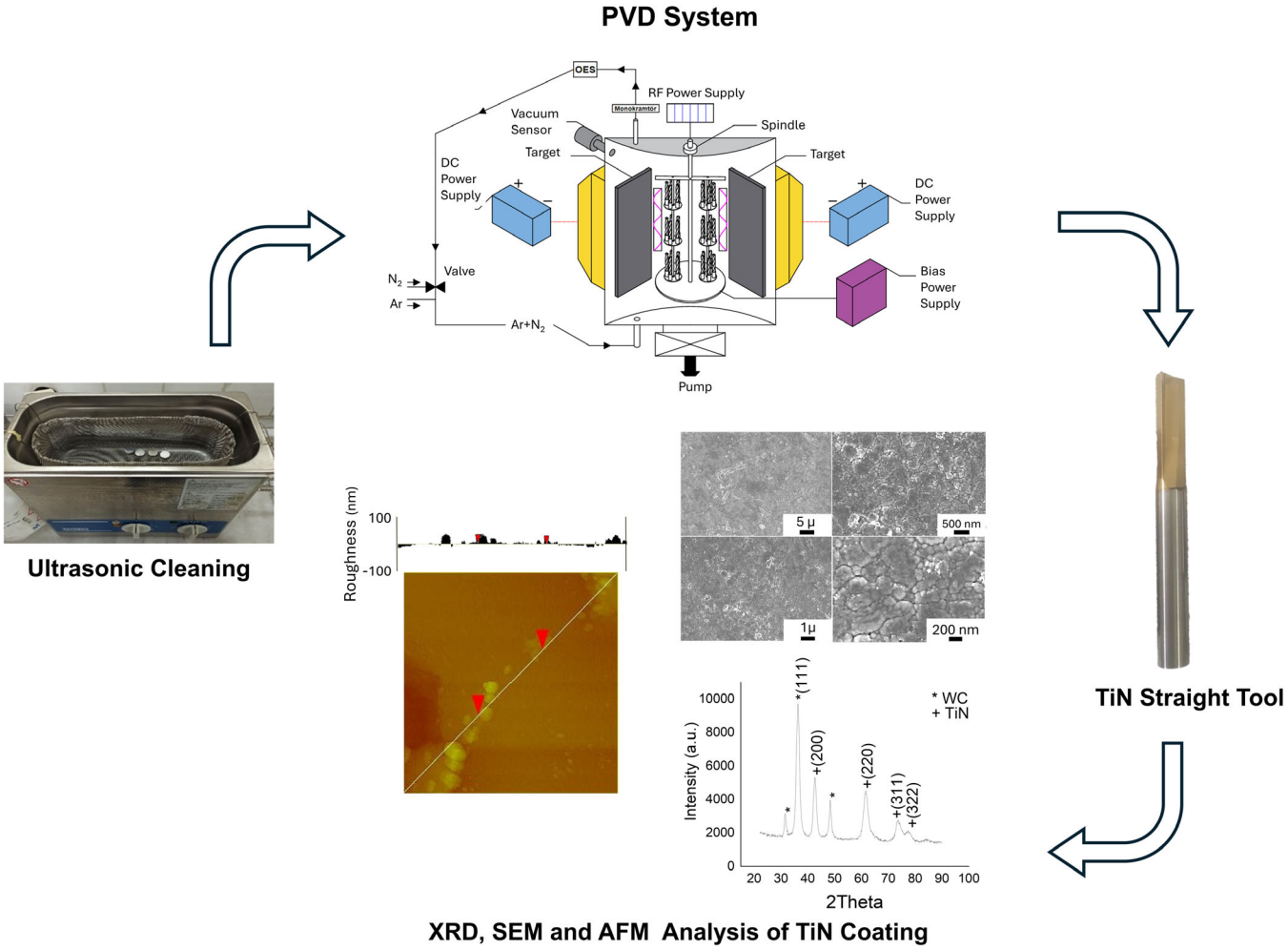

FIGURE 2 TiN thin film deposition and the schematics of characterization. AFM, atomic force microscopy; EDX, energy dispersive x-ray spectroscopy; SEM, scanning electron microscopy; XRD, x-ray diffraction.

TABLE 2 Sputtering parameters for titanium nitride coating of end mills.

Parameters	Values
Target power (W)	4000
Bias (−V)	80
Ar flow (sccm)	20
N_2 flow (sccm)	8
Working Pressure (mTorr)	2

and set to 50%. OES enabled the argon/nitrogen gas ratio to be controlled to achieve the desired plasma density at a specific wavelength.[49]

During the deposition process, bias voltage was provided to the substrates using a second DC source. First, the target and then the substrates were cleaned in plasma medium. Before the nitride coating, an intermediate metallic layer (Ti) was deposited to increase adhesion and create a compatible interface between the tool material and coating. During the procedure, the substrates were passed in front of the target at a controlled rotational speed. Table 2 lists the deposition parameters of the TiN coating obtained in this study.

Analyzes were performed to reveal the structure and properties of the obtained TiN thin films. The surface morphology and microstructure of TiN thin films were examined by scanning electron microscope (SEM) at various magnifications, and their elemental composition was determined by energy dispersive x-ray spectroscopy (EDX). X-ray diffraction (XRD) analysis was performed for the crystal structure and orientations, and the surface topography and nanoscale roughness of the films were determined by atomic force microscopy (AFM). To determine the mechanical properties of TiN thin films, their hardness was measured using the CSEM nanohardness device.

2.3 | Experimental setup and design

A 40 × 70 mm samples were machined on a three axis CNC mill (Hannsa YL1000B) to form the plates. They were then labeled with numbers from 1 to 54. One side of the samples was machined by conventional milling and the other side by climb milling. The side that is machined by conventional milling is shown with an arrow pointing toward that side of the rectangular piece for the sake of discernibility. To provide a constant width of cut, samples were machined from all sides with a 6 mm coated pyramid carbide end mill (DIN6535 HA type nACo) with a cutting depth of

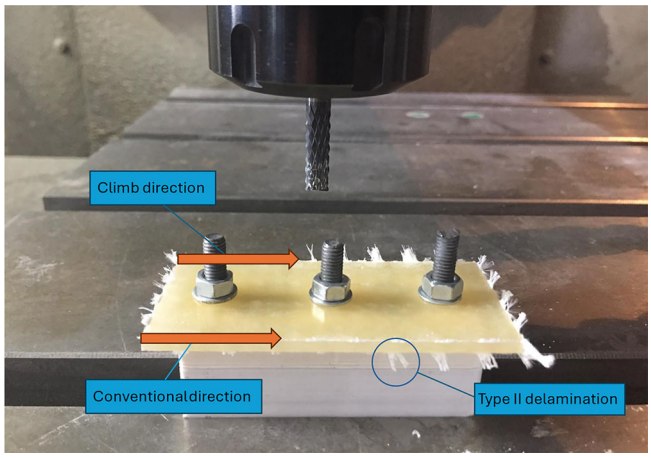

FIGURE 3 Experimental setup.

1.5 mm, spindle speed of 1000 rpm and feed rate of 0.1 mm/rev. Every sample was machined with conventional and climb milling methods, from each long side of the rectangular sample. A visual regarding the cutting directions is provided in Figure 3. Samples machined with three different tools with a cutting width of 2.5 mm. The experimental setup can be seen in Figure 3.

During the edge milling of BFRP and S2-GFRP samples, different machining variables are tested to determine the optimum values. These variables include cutting speed, feed rate, drilling bit type, and coating are listed in Table 3.

2.4 | Taguchi method

Taguchi method assumes that the signal-to-noise (S/N) ratio of a set of data where signal is desired and noise is not desired, it is possible to determine the individual effects of parameters on the outcome. Taguchi analysis gives the output in the form of delta value, which is the difference in best and worst results to see the improvement with the optimized parameters. The value of burr area also holds a crucial part of the analysis. Taguchi design implements different variations of equations whether the outcome for the value of signal-to noise ratio is optimal when it is large, small, or nominal. Since smaller burr area and length are desired in the analysis, smaller is better formulation is applied to the data, which is shown in Equation (1).

$$\frac{S}{N_{LB}} = -10\log 10\left(\frac{1}{r}\sum\nolimits_{i=1}^{r} R_i^2\right). \quad (2)$$

In the Taguchi analysis for machining S2-GFRP and BFRP, factors such as cutting speed, feed rate, milling

Parameters	Level 1	Level 2	Level 3
Tool surface	Uncoated	Coated	-
Tool type	Helical carbide	Straight carbide	Helical HSS
Cutting speed (rev/min)	500	1000	1500
Feed (mm/rev)	0.050	0.100	0.150

TABLE 3 Factors and levels in the experimental tests.

TABLE 4 Taguchi L18 design and corresponding material removal rates.

Test no.	Tool surface	Tool type	Spindle speed	Feed rate	MRR (mm^3/min)	
					S2-GFRP	BFRP
1	1	1	1	1	169	225
2	1	1	2	2	675	900
3	1	1	3	3	1519	2026
4	1	2	1	1	169	225
5	1	2	2	2	675	900
6	1	2	3	3	1519	2026
7	1	3	1	2	338	450
8	1	3	2	3	1013	1350
9	1	3	3	1	506	676
10	2	1	1	3	506	676
11	2	1	2	1	338	450
12	2	1	3	2	1013	1350
13	2	2	1	2	338	450
14	2	2	2	3	1013	1350
15	2	2	3	1	506	676
16	2	3	1	3	506	676
17	2	3	2	1	338	450
18	2	3	3	2	1013	1350

Abbreviations: BFRP, basalt fiber reinforced plastics; S2-GFRP, S2-glass fiber reinforced plastics.

tool type, and coating were varied at various levels to study their effects on cutting performance. The cutting speed levels were low (500 rpm), medium (1000 rpm), and high (1500 rpm), while feed rate levels were set at low (0.050 mm/rev), medium (0.100 mm/rev), and high (0.150 mm/rev). Since it is a novel analysis, levels are selected to cover a wider range of cutting speed and feed rate combinations compared with the literature. Three tool types (helical HSS, straight flute carbide, and helical carbide) were used at varying levels. Coating was applied at two levels: coated and uncoated. The experiments were designed using a Taguchi L18 orthogonal array (Table 4), which allowed for the reduction of the total number of experiments to 18 while ensuring a comprehensive exploration of the parameter space. Material removal rate (MRR) for the experiments is calculated for both materials and listed in Table 4. Analysis of the results including the burr area will provide insights into the optimal machining conditions for these composites. The results will be combined with an analysis of variance (ANOVA) for individual significance of parameters.

Each experiment was meticulously conducted three times with precisely identical parameters to ensure the consistency and reliability of the results. Notably, no damage or cracks were observed on the milling tools at the macro scale, indicating their durability and suitability for the machining process. To facilitate clear identification and comparison, one side of the composite samples was machined using conventional milling techniques, while the other side was machined using climb milling. These sides were marked with test numbers and an arrow pointing to the side machined by conventional milling, enhancing the discernibility of the machining methods employed.

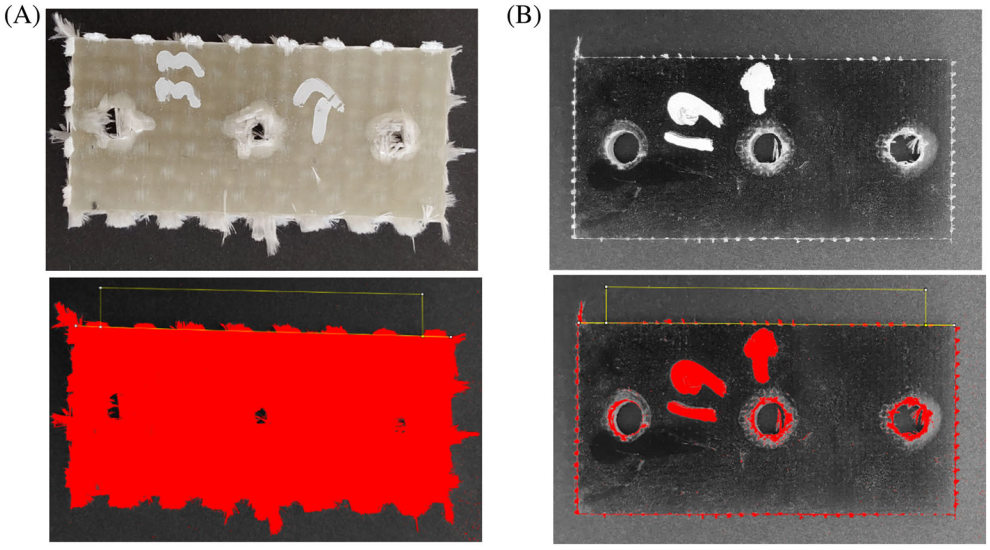

FIGURE 4 (A) S2-glass fiber reinforced plastics and (B) basalt fiber reinforced plastics samples converted into colored burrs after the milling operations.

2.5 | Burr analysis

The machined samples were examined under a camera (Sony IMX355) with a 28 mm lens, and images are taken to determine the extent of fiber length and total burr area. The images are then converted into 32 bit and color threshold is set manually in order to separate the burrs from the main body of composite plates as shown in Figure 4. The acquired images were then used to measure the area of the protruding fibers using the ImageJ program.[50] The program uses the contrast difference between the burr and the base material to accurately measure the burr area. A predetermined rectangular shape, with a set distance of 5 mm from the edges, is adjusted to fit the edge of the sample and cover the burrs. The shape is adjusted to cover the entire area of fringes perpendicular to the base. The program analyzes the particles that have lighter colors and calculates the area fraction of colored particles in the selected polygonal area as shown in Figure 4.

2.6 | Desirability analysis

A desirability analysis is conducted to calculate a desirability index to discuss the effect of MRR and burr area. Milling parameter combinations with low spindle speed and feed rate may be beneficial for burr area and burr length. However, the practical application of composite milling in the industry requires the process to be fast as it is effective in order to gain an advantage in the competitive environment. Therefore, MRR is used as a parameter that refers to the speed of the operation. High MRR and low burr area is desired since faster machining with similar burr area saves time from the operations without compromising the burr area. Desirability index calculated separately for MRR and burr area starting by normalization of data. Desired normalization values can be calculated as:

$$d_{\mathrm{MRR}} = \frac{x - \min(X)}{\max(X) - \min(X)}, \tag{3}$$

$$d_{\mathrm{burr}} = 1 - \frac{x - \min(X)}{\max(X) - \min(X)}, \tag{4}$$

where x represents the data for MRR and burr area, $\min(X)$ and $\max(X)$ represents minimum and maximum value of chosen dataset, respectively. Composite desirability is calculated as:

$$D = \sqrt{(d_{\mathrm{burr}} * d_{\mathrm{MRR}})}. \tag{5}$$

In this analysis, desirability of MRR and burr area is equally weighted thus implies that the significance of high MRR and low burr area is equal.

3 | RESULTS AND DISCUSSION

In this section, the results of the experimental investigation on BFRP and S2-GFRP are presented. The results are organized according to three key aspects explored in the study, which are the coating characterization, area, and length analysis of burrs with ImageJ, and Taguchi analysis based on the machining parameters.

3.1 | Characterization of coated thin films

The properties of TiN thin films produced by reactive magnetron sputtering technique depend on the

deposition process parameters, such as target power, reactive gas ratio, and working gas pressure.[49] Controlling the deposition parameters allows customization of the thin film microstructure and properties. In this study, the microstructure, grain size, and crystal structures of the TiN films obtained depending on the selected process parameters were characterized.

Figure 5 shows the microstructure and surface morphology of the TiN coating layer. SEM images taken at different magnifications highlight TiN coatings on WC-10%Co and HSS-E substrates. The TiN film on the WC-10%Co substrate reveals a highly dense, uniform cauliflower-shaped structure (Figure 5A). It has high integrity, free of discontinuities on the entire surface. The magnetron sputtering method allows obtaining very thin, dense TiN microstructures.[49] On the HSS-E substrate (Figure 5B), the TiN coating surface has high homogeneity, although it exhibits visible grain boundaries, pores, and voids compared with carbide substrates. The presence of nitrogen and titanium detected in the EDX analysis confirms the formation of TiN coating with the determined N and Ti atomic composition values. The N/Ti ratio in the film shows an increasing trend with the increase of the N_2/Ar ratio. At the same time, lower N_2/Ar ratio is effective both on orientation and in obtaining denser microstructures.[43]

XRD patterns of TiN thin films were analyzed with TiN (111), (200), and (220) planes exhibiting the most intense peaks. The analysis results (JCPDS-ICOD: 38-1420), which can be seen in Figure 6, confirmed the compatibility with TiN. In particular, the TiN(111) orientation at an angle value of 2θ 36.280 emerged as the dominant peak in thin films deposited by sputtering in a DC magnetic field.[51–53] The second strong peak was in the (200) direction at 2θ 42.590 angle value, and these strong peaks showed that the TiN coating mainly grew in the (111) and (200) directions and had a crystal structure. As seen in Figure 6, TiN(111) orientation on different substrates revealed similar peak feature, consistent with the literature.[51] The weaker peaks in the TiN coating are observed at the (200) plane and (311) plane, respectively.

Average crystallite size (Figure 7A) was determined using the Scherrer formula (Equation (5)),

$$D = \frac{0.9x\lambda}{\beta x \cos\theta}, \tag{6}$$

where β represents the width at half maximum of the diffraction line, θ signifies the Bragg angle, and λ denotes the wavelength.

Nitrogen atoms located in the lattice interspaces within the microstructure significantly affect the

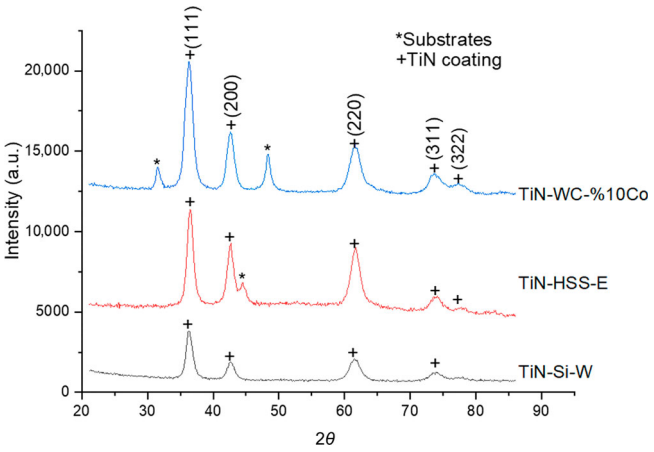

FIGURE 6 X-ray diffraction patterns.

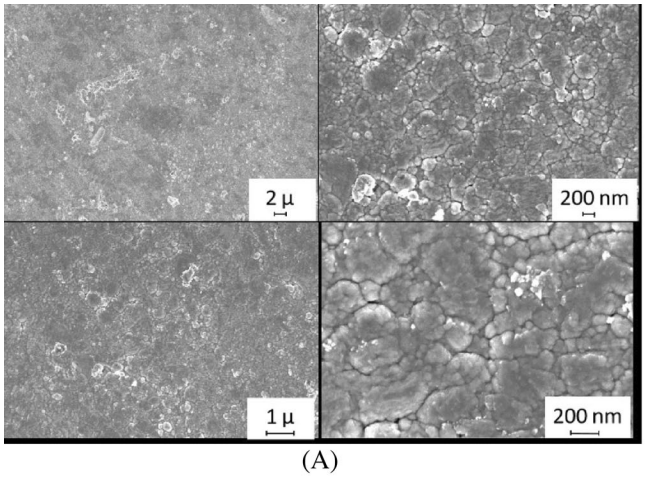

FIGURE 5 (A) Scanning electron microscopy (SEM) image of TiN coating on WC 10%Co and (B) SEM image of TiN coating on high-speed steel (HSS).

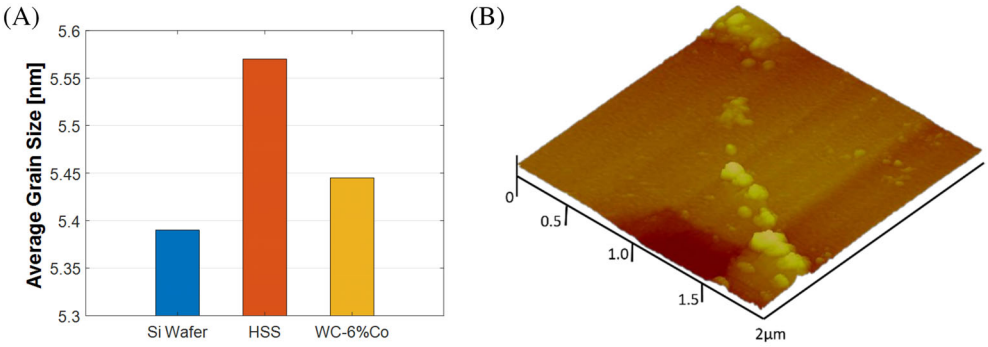

FIGURE 7 (A) Grain size of TiN thin films on substrates and (B) atomic force microscopy (AFM) analysis.

hardness of TiN thin films. The N_2/Ar ratio, which is effective on stoichiometry, affects both crystallite size and hardness value. Considering that TiN coating is applied to milling tools, the hardness of the tools plays a very important role in operational performance. Hardness tests were carried out using the CSM Instrument brand nanohardness tester, and hardness values of 2238 and 1672 HV were measured for WC-10%Co and HSS-E coatings, respectively. The relatively low hardness of HSS-E thin films can be attributed to the crystallite size and voids in the film morphology. The high hardness value observed in the hardness tests of TiN coatings deposited on the WC-10%Co substrate increases due to the low crystallite size. It is emphasized in the literature that grain sizes and voids have an impact on general hardness properties.[43]

Smoother tool surfaces are highly desirable in composite milling due to the less friction and heat generation at the cutting edge, which helps prevent thermal damage to both the tool and composite material as it can degrade the composite matrix and lead to poor surface finish or dimensional inaccuracies.[54] Moreover, composite materials tend to produce chips that can be difficult to evacuate due to their fibrous nature.[55] Decreasing the surface roughness of milling tools (i.e., coating of the end mills with TiN) reduces chip adhesion and buildup on the tool, improving machining efficiency and reducing the risk of chip recutting, which can affect surface quality of the fabricated composite plates.[55] Due to the less burr formation, smooth tool coatings contribute to maintaining precise dimensional tolerances, ensuring consistency and quality in the manufactured components. These benefits collectively contribute to efficient and effective machining of composite materials across various industrial applications.[56] The surface hardness of thin films depends on the surface roughness of the substrate materials. Rough surfaces with micro voids cause hardness values to decrease.[43] In this study, the surface roughness of TiN coating was examined by AFM and shown in Figure 7B. AFM images show that the TiN film surface obtained after coating is relatively smooth and dense, and exhibits a budded structure with upward needle-like protrusions. As a result of AFM analysis, the average roughness value of the TiN film layer was determined as 5.26 nm (Figure 7B).

Another parameter affecting the hardness in the magnetron sputtering method is the bias voltage applied during deposition, and determining the critical bias voltage is very important.[51,57,58] In this study, TiN coating was obtained at −80 V as the critical bias voltage. At very high bias values, the mobility of the atoms increases, and the grains become coarser. High bias voltage increases the lattice stress due to the increase in ion impingement, thus leading to decreased hardness due to residual stresses.[46]

3.2 | Milling-induced damage analysis

Image analysis is made by calculating the mean burr area and burr length values of three repeats of each parameter combination. More burr area is observed from S2-GFRP compared with BFRP. An observation of Figure 8 reveals that whether it is coated or not, and regardless of cutting parameters, HSS tools (test numbers 7, 8, 9 for uncoated, 16, 17, 18 for coated) result in the highest burr area.

Although coating changes the surface properties of the tool significantly, cutting quality, evaluated by the burr area and length, does not change considerably. A comparison between BFRP and S2-GFRP shows that BFRP shows significantly less burr area compared with S2-GFRP, regardless of the difference in thickness. In most cases, the conventional cutting method demonstrates less burr area than climb cutting. Moreover, the standard deviation for the samples machined with HSS is significantly higher for both burr length and burr area calculations, due to the formation of irregular burrs as shown in Figure 9. Due to the poor mechanical properties of HSS material, the cutting forces developed in the fiber-tool interface are insufficient to cut the fibers, therefore fibers are either entangled to the tool instead of

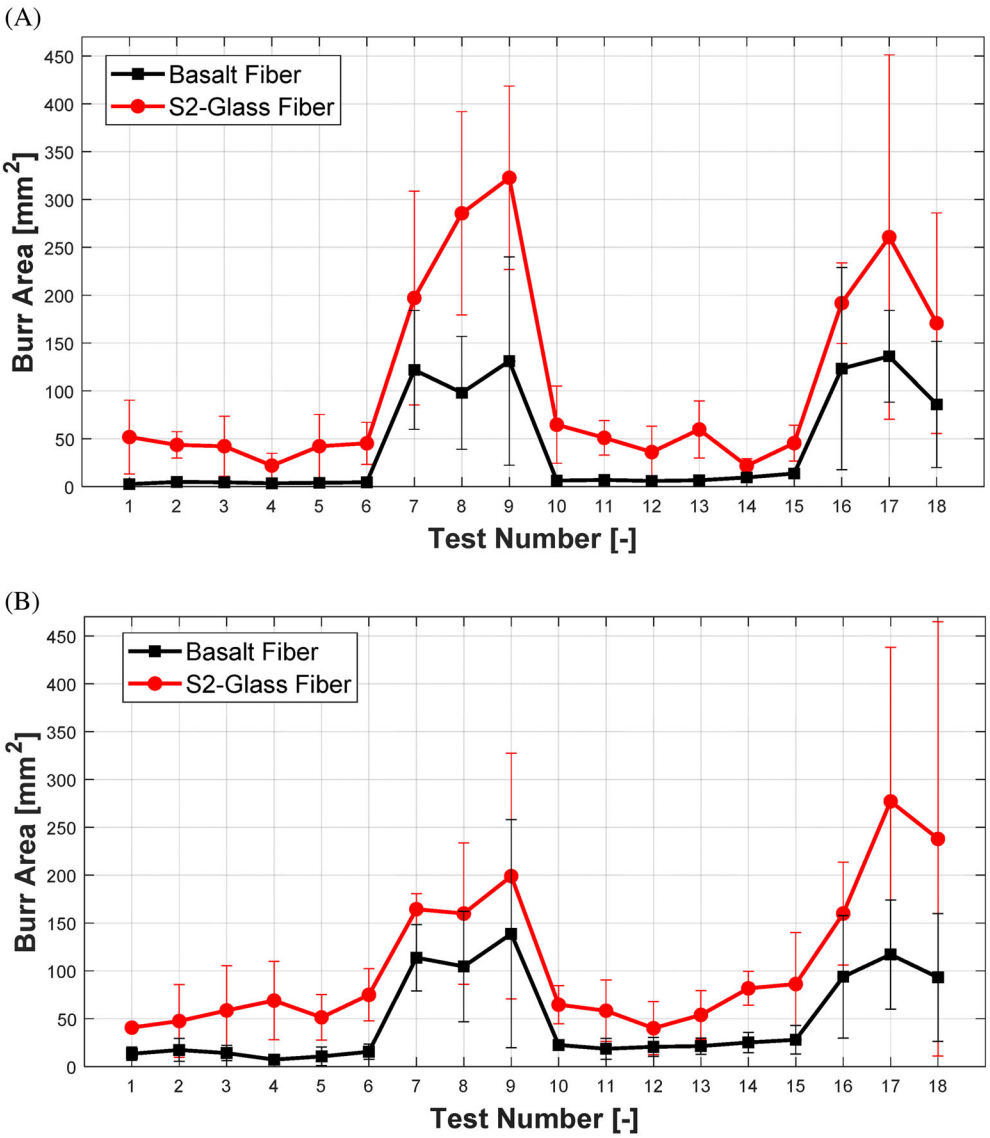

FIGURE 8 Burr area in (A) conventional and (B) climb milling of S2-glass fiber reinforced plastics (S2-GFRP) and basalt fiber reinforced plastics.

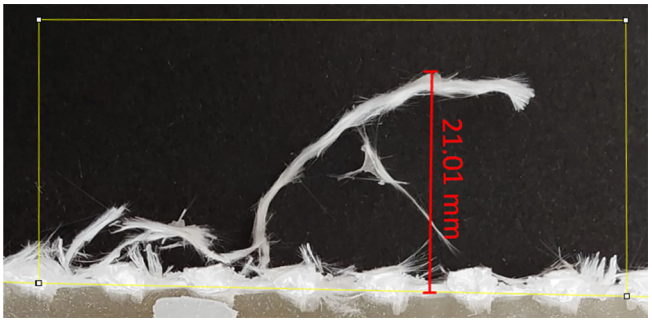

FIGURE 9 Measurement of the length of an irregular burr.

being cut or form burr clusters, resulting in a high burr area.

Burr length is calculated in a similar fashion. The mean value of three repetitions for each parameter is calculated. Comparing S2-GFRP and BFRP, it is evident that S2-GFRP samples exhibit a greater burr length. Referring to Figure 9, irrespective of coating or cutting parameters, HSS tools consistently yield the longest burr lengths. Despite significant alterations in surface properties due to coating, there is minimal change in cutting quality, as assessed by burr length. Notably, BFRPs consistently display shorter burr lengths in comparison to S2-GFRPs. Additionally, conventional cutting methods generally result in shorter burr lengths than climb cutting across various scenarios. The overall trend of burr area and burr length graphs shown in Figures 8 and 10 align with each other, for both S2-GFRPs and BFRPs.

The influence of factors such as cutting speed, feed rate, tool geometry, and tool surface quality (i.e., surface roughness and coating type) on the machining performance in fiber reinforced composites has been

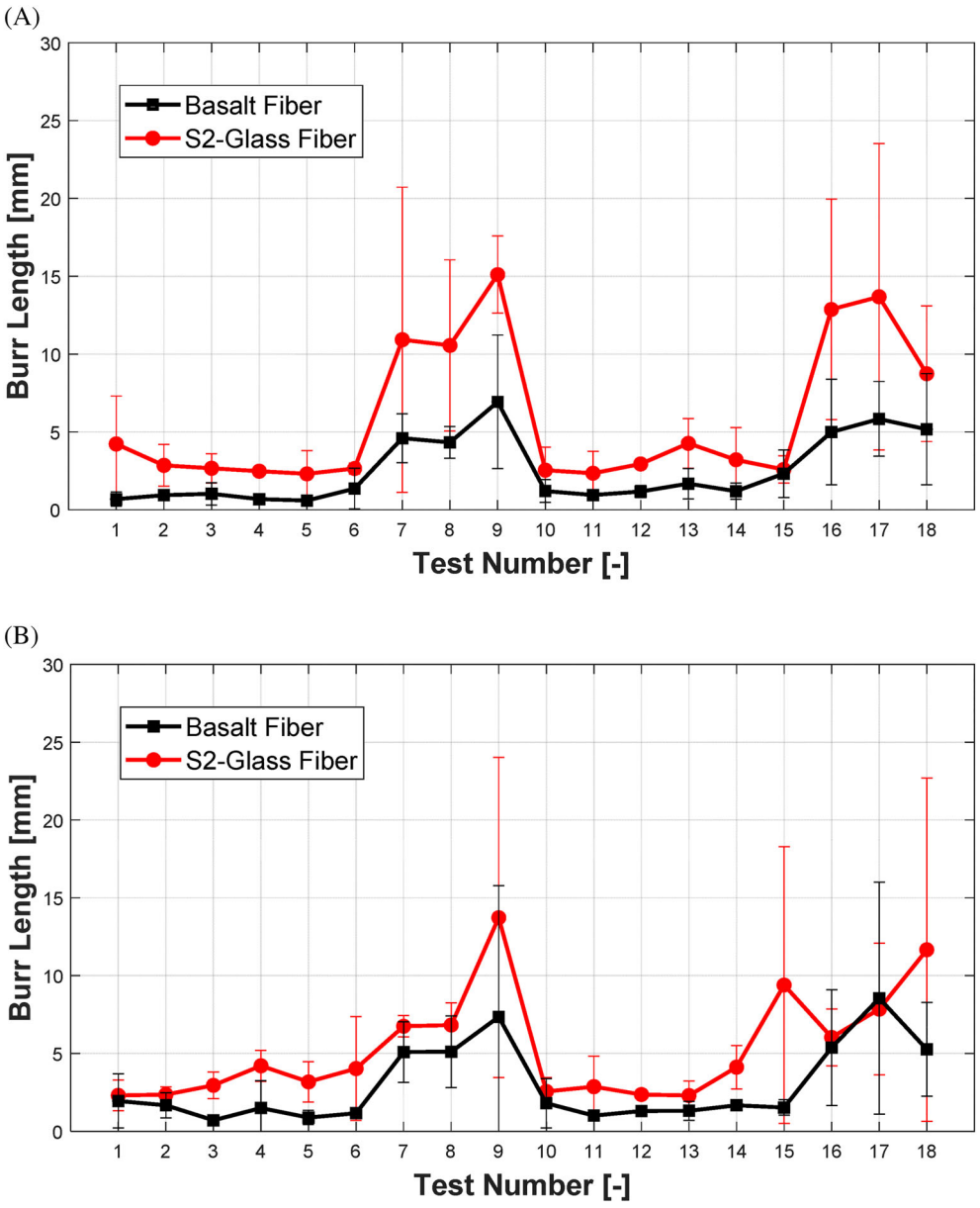

FIGURE 10 Maximum burr length for (A) conventional and (B) climb cutting for S2-glass fiber reinforced plastics (S2-GFRP) and basalt fiber reinforced plastics.

investigated in previous researches.[59–61] As experiments 1–9 and 10–18 are performed with uncoated and coated cutting tools, respectively (Table 4), it can be clearly seen in Figures 8 and 10 that coating of the HSS and carbide end mills with TiN has small effect on the burr size in milling of S2-GFRP and BFRP composites. However, in literature, the presence of thin TiN films has significantly reduced the wear rate of the cutting tools due to its greater mechanical properties than the HSS and tungsten carbide materials during machining various composite substrates.[62,63] Although, the high hardness in TiN-coated WC-10%Co samples is assumed to provide a desirable burr formation as it makes the cutting edge geometry more resistant to composite components,[64] the effect of coating has negligible on burr formation in this study (Figures 8 and 10).

It is stated in the literature that TiN-coated carbide tools perform well at high cutting speeds and feed rates up to 0.15 mm/tooth feed rate in the processing of CRFP samples. However, if working at a feed rate of 0.25 mm/tooth, it is stated that the increase in surface roughness reaches values considered high for aviation applications.[61] For this reason, the effect of TiN-coated tools on the burr area can be attributed to surface processing parameters.[61] The findings emphasize the significant role of feed rate as one of the foremost factors influencing surface roughness in the processing of composite materials.[65] Therefore, meticulous analysis of both cutting parameters and tool geometry is imperative for each composite material.

Given the distinct nature of composite material milling from other materials,[39] our study provides researchers

with an opportunity to advance their understanding of milling S2-GFRP and BFRP composites using both coated and uncoated tools. Determining appropriate cutting tools and conditions for milling S2-GFRP and BFRP composites can be optimized as a new approach in terms of burr length and area.

3.3 | Taguchi analysis

Taguchi analysis performed on BFRP and S2-GFRP composites revealed valuable information regarding the effects of various process parameters on the quality characteristics of the burr areas. It is important to note that the delta values change with the cutting direction and sample material for parameters other than tool type. It can be observed from Figure 11A,B that the same parameters used for conventional and climb cutting directions yield different results. One of the main reasons for this phenomenon is the forces acting on the tool-material interface are different for conventional and climb cutting. A comparison between length and area of BFRP and S2-GFRP in both Figures 11 and 12 reveal a matching overall pattern for corresponding signal-to-noise ratios.

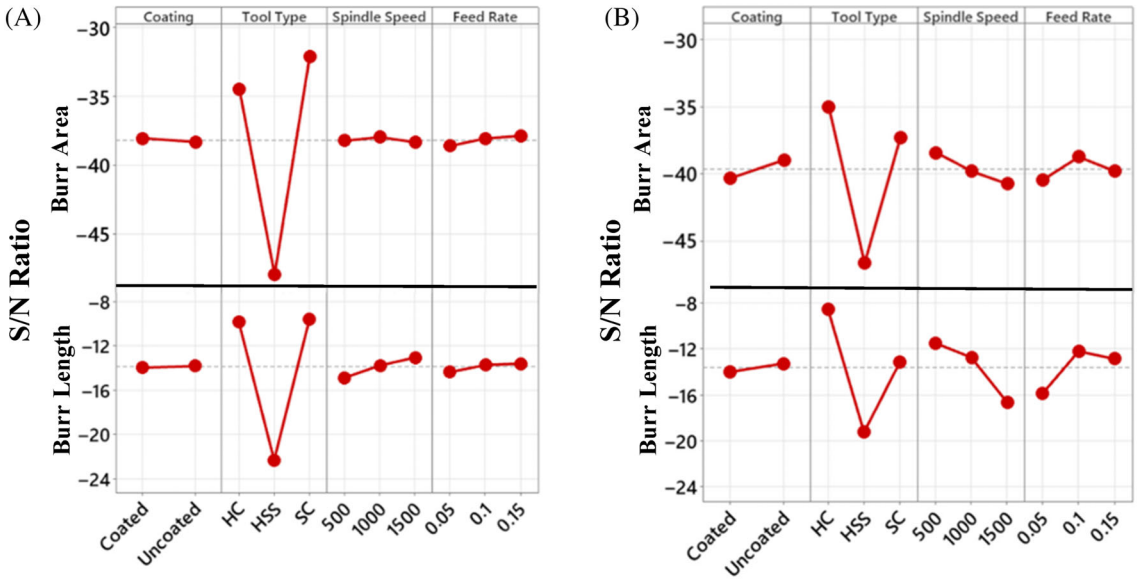

FIGURE 11 Signal-to-noise ratios for burr areas and lengths in (A) conventional and (B) climb S2-glass fiber reinforced plastics milling.

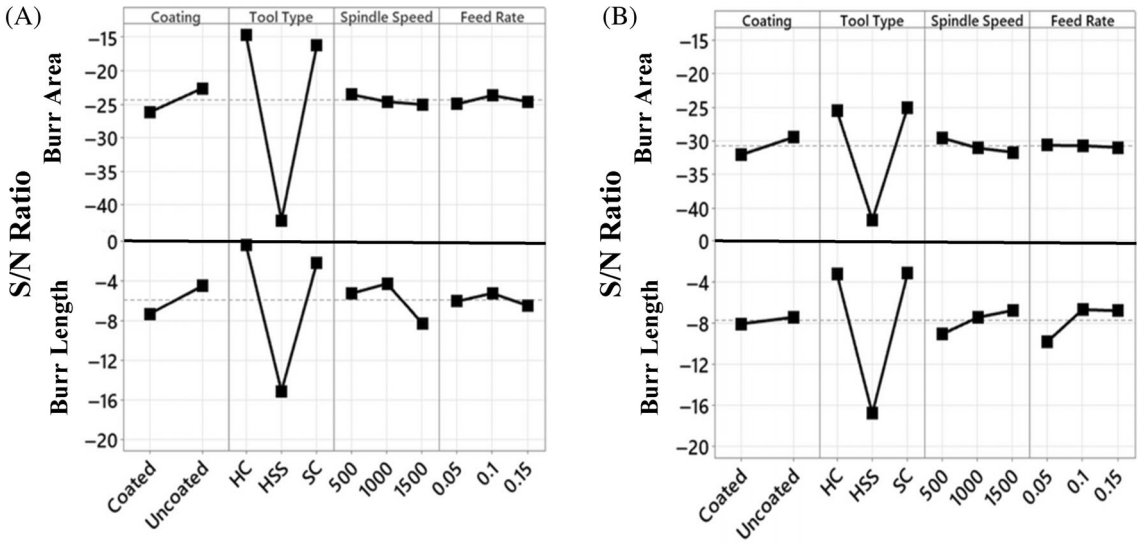

FIGURE 12 Signal-to-noise ratios for burr areas and lengths in (A) conventional and (B) climb basalt fiber reinforced plastics milling.

Tool material is the dominant factor in both milling directions, for both burr area and burr length calculations. Spindle speed and feed rate parameters have a more significant effect on burr area when combined with climb milling, compared with conventional milling. Burr area and burr length of corresponding materials and milling directions generally align well, indicating stability of data.

Figure 11 shows the S/N ratios of S2-GFRP samples for burr area and burr length with conventional and climb milling. Coating data, although not significant, tends to show better results with uncoated tools, except for burr area with conventional milling. Straight carbide shows higher level of influence to both burr area and burr length in conventional milling, while helical carbide shows superiority with climb milling. While higher-is better is evidently the trend in conventional milling for spindle speed and feed rate parameters in Figure 11A, highest and lowest parameters of feed rate and higher spindle speed show considerable decrease in performance in climb milling in Figure 11B.

Figure 12 shows the S/N ratio of BFRP samples. Uncoated tools show superiority for both milling directions, and both burr area and burr length analyses. Helical carbide tool shows better results for conventional milling direction in Figure 12A, while straight carbide tool shows better performance in climb milling direction in Figure 12B. Middle parameters result with highest S/N values for conventional milling for BFRP. Burr area for climb milling shows improved results with lower spindle speed and feed rate parameters, while burr length is the lowest with higher spindle speed and feed rate, as it can be seen in Figure 12B. It is important to note that the optimum parameters for different milling directions for S2-GFRP and BFRP are the opposite of each other, meaning that the optimum parameters for climb milling of S2-GFRP evidently aligns well with the conventional milling of its basalt counterpart, and vice versa.

ANOVA revealed the relevance of the parameters to the results. The analysis was conducted with Minitab® Statistical Software for the level of significance of 5% and a level of confidence of 95%. Conventional and climb cutting data is merged for this analysis. The results can be seen in Tables 5 and 6. An ANOVA table consists of various parameters. Source of variation refers to different sources of variation. Degrees of freedom (DF) refers to several independent variables for a parameter minus one. Sequential sums of squares (Seq SS) refer to the variation of different components depending on the order, while adjusted sums of squares (Adj SS) refers to the variation without taking the order of the measurements into account. Since the analysis is a one-way ANOVA, which is based on the means of the data, the values of Adj SS and Seq SS are equal, and the order of data and the experiments are not important. Adjusted mean squares (Adj MS) refers to the number of variations that are available to be explained by model, regardless of the order. Adj MS value also considers the degree of freedom while Adj SS does not. *F*-value is the test to measure the association of the data with the response. *F* value is then used to calculate the *p*-value. *p*-value refers to the statistical significance of how strongly the parameter rejects the null hypothesis. A strongly rejected null hypothesis is referred as a low *p*-value, meaning a strong correlation between the parameter and the response *p*-value below

TABLE 5 ANOVA for means of the milling induced damages for S2-glass fiber reinforced plastics composites.

Source of variance	DF	Seq SS	Adj SS	Adj MS	*F*	*p*
Burr area						
Coating	1	27	27	26.5	0.06	0.813
Tool type	2	111,259	111,259	55629.7	123.42	0.000
Spindle speed	2	1486	1486	743.0	1.65	0.241
Feed rate	2	2508	2508	1253.9	2.78	0.110
Residual error	10	4508	4508	450.8		
Total	17	119,787				
Burr length						
Coating	1	0.069	0.069	0.069	0.07	0.801
Tool type	2	207.641	207.641	103.820	100.29	0.000
Spindle speed	2	8.047	8.047	4.023	3.89	0.056
Feed rate	2	11.071	11.071	5.535	5.35	0.026
Residual error	10	10.352	10.352	1.035		
Total	17	237.179				

TABLE 6 ANOVA analysis of the milling induced damages for basalt fiber reinforced plastics.

Source of variance	DF	Seq SS	Adj SS	Adj MS	*F*	*p*
Burr area						
Coating	1	8.1	8.1	8.1	0.06	0.808
Tool type	2	40944.3	40944.3	20472.2	158.38	0.000
Spindle speed	2	9.2	9.2	4.6	0.04	0.965
Feed rate	2	300.1	300.1	150.1	1.16	0.352
Residual error	10	1292.6	1292.6	129.3		
Total	17	42554.3				
Burr length						
Coating	1	0.4622	0.4622	0.4622	1.10	0.319
Tool type	2	79.3998	79.3998	39.6999	94.49	0.000
Spindle speed	2	0.4081	0.4081	0.2041	0.49	0.629
Feed rate	2	2.4912	2.4912	1.2456	2.96	0.097
Residual error	10	4.2014	4.2014	0.4201		
Total	17	86.9628				

TABLE 7 Individual and composite desirability of burr area and material removal rate (MRR).

Material	S2-GFRP						BFRP					
Direction	Conventional			Climb			Conventional			Climb		
Desirability	d_{Burr}	d_{MRR}	*D*	d_{Burr}	d_{MRR}	*D*	d_{Burr}	d_{MRR}	*D*	d_{Burr}	d_{MRR}	*D*
1	0.900	0.000	0.000	0.998	0.000	0.000	1.000	0.000	0.000	0.953	0.000	0.000
2	0.927	0.375	0.590	0.969	0.375	0.602	0.983	0.375	0.607	0.923	0.375	0.588
3	**0.932**	**1.000**	**0.965**	**0.922**	**1.000**	**0.960**	**0.985**	**1.000**	**0.993**	**0.948**	**1.000**	**0.974**
4	0.999	0.000	0.000	0.878	0.000	0.000	0.993	0.000	0.000	1.000	0.000	0.000
5	0.932	0.375	0.591	0.952	0.375	0.597	0.990	0.375	0.609	0.974	0.375	0.604
6	**0.922**	**1.000**	**0.960**	**0.853**	**1.000**	**0.924**	**0.985**	**1.000**	**0.993**	**0.938**	**1.000**	**0.969**
7	0.417	0.125	0.229	0.475	0.125	0.244	0.106	0.125	0.115	0.190	0.125	0.154
8	0.123	0.625	0.278	0.495	0.625	0.556	0.285	0.625	0.422	0.260	0.625	0.403
9	0.000	0.250	0.000	0.330	0.250	0.287	0.037	0.250	0.096	0.000	0.250	0.000
10	0.857	0.250	0.463	0.896	0.250	0.473	0.972	0.250	0.493	0.883	0.250	0.470
11	0.903	0.125	0.336	0.923	0.125	0.340	0.968	0.125	0.348	0.915	0.125	0.338
12	0.952	0.625	0.772	1.000	0.625	0.791	0.974	0.625	0.780	0.899	0.625	0.749
13	0.874	0.125	0.331	0.942	0.125	0.343	0.970	0.125	0.348	0.894	0.125	0.334
14	1.000	0.625	0.791	0.824	0.625	0.718	0.947	0.625	0.769	0.864	0.625	0.735
15	0.921	0.250	0.480	0.806	0.250	0.448	0.916	0.250	0.479	0.843	0.250	0.459
16	0.435	0.250	0.330	0.495	0.250	0.351	0.095	0.250	0.155	0.342	0.250	0.293
17	0.206	0.125	0.161	0.000	0.125	0.000	0.000	0.125	0.000	0.165	0.125	0.143
18	0.505	0.625	0.562	0.166	0.625	0.322	0.376	0.625	0.485	0.347	0.625	0.466

Abbreviations: BFRP, basalt fiber reinforced plastics; S2-GFRP, S2-glass fiber reinforced plastics.

0.05 would be strongly associated with the result, between 0.05 and 0.1 would be a rather weak correlation, and a *p*-value greater than 0.1 would mean that the correlation is statistically insignificant. The model is considered to be valid if there is at least one parameter with $p \leq 0.05$. Table 5 contains information regarding

the statistical significance of the machining parameters with respect to the burr area and burr length for S2-GFRP composites Tool type, with a *p*-value of 0.000, has the highest significance to both burr area and burr length. Feed rate, while showing a slightly out of the range of significance with a *p*-value of 0.110 for burr area, is a defining factor for burr length with a *p*-value of 0.031. Spindle speed is out of the range of significance for burr area, while being relevant for burr length with a *p*-value of 0.056 referring to a weak correlation. *p*-value of coating is far out of the range of relevance for both burr length and burr area for both materials.

The overall trend for BFRP matches the ANOVA for S2-GFRP. Similar to S2-GFRP, Table 6 reveals that *p*-value for coating can be considered as statistically insignificant, while tool type has the strongest influence. BFRP differs with resulting the highest *p*-value for spindle speed with 0.965 for burr area while consistently being irrelevant for burr length. Feed rate has a somewhat decent influence on burr length with a *p*-value of 0.097, however irrelevant to burr area with a *p*-value of 0.352. Analysis for both materials along well for coating, tool type and feed rate. Spindle speed showed significant effect on S2-GFRP samples while being the most irrelevant parameter of BFRP samples for both burr length and burr area.

A desirability analysis is conducted to select the cutting parameters with the highest MRR with lowest burr area. The desirability analysis provides valuable insights into the performance of the machining process based on two critical parameters: burr area and MRR. The desirability scores have been normalized to facilitate comparison, with lower burr area and higher MRR values considered more desirable. By considering both burr area and MRR simultaneously, the composite desirability metric enables a comprehensive evaluation of machining outcomes, aiding in decision-making processes aimed at optimizing process parameters for enhanced productivity and quality. The results of desirability analysis can be seen in Table 7. The most desirable results according to the analysis are, regardless of milling direction and sample material, are with the test number 3 and 6 (highlighted in bold), corresponding to uncoated helical carbide and uncoated straight carbide respectively with both having spindle speed of 1500 rpm and feed rate of 0.15. While test number 12 and 14 shows significant d_{Burr} value, the MRR of the samples are considerably low, therefore displays low desirability.

4 | CONCLUSION

This study presents a comprehensive analysis of cutting performance in machining S2-GFRP and BFRP composites to have a deeper understanding of milling factors, such as tool material, tool geometry, cutting direction, cutting speed, and feed rate on the quality of the machining process. Burr areas and burr lengths of S2-GFRP and BFRP composites are selected as parameters as an indicator of milling quality, and total burr area and burr length calculation with a novel usage of image analysis method is implemented to the study. HSS end mills resulted with the highest burr area and burr length in every analysis, with inferior cutting quality, suggesting the unsuitability of HSS tools for the machining of S2-GFRP and BFRP. This finding is reinforced by eliminating the contribution of tool angles, since helical carbide tool is modeled after its HSS counterpart.

While conventional milling consistently yields lower burr area values compared with climb milling, particularly due to the removal of burrs as a structural cluster, conventional milling may pose challenges in the context of longer samples, potentially leading to the entanglement of excess string-like burrs.

Taguchi analysis is conducted to calculate S/N ratios of coating, tool type, spindle speed, and feed rate. Among the parameters, tool type has the highest delta value in both conventional and climb milling directions, for both burr area and burr length analyses. For S2-GFRP composites, uncoated straight carbide tool showed better suitability for burr area of conventional milling while uncoated helical carbide showed better results for burr length with climb milling. While the difference is insignificant in BFRPs, the better parameters are the opposite of S2-GFRPs, being conventional helical carbide showing better results for conventional milling as straight carbide showing better results with climb milling for both burr area and burr length parameters. ANOVA results suggest that the effect of coating is irrelevant to the burr area for most parts of the analysis, while spindle speed and feed rate are relevant for specific cutting direction and composite material combinations. An equal-weighted desirability analysis where low burr area and high MRR is desired is conducted. Highest MRR parameter combination of spindle speed of 1500 and feed rate of 0.15 is resulted as the parameters with highest desirability.

Future research endeavors may further explore the interactions between tool parameters, material properties, temperature effects, and machining conditions. The difference of optimum parameters for BFRP and S2-GFRP composites suggests that the parameter combination is required to be tailored for different composite materials. Such endeavors hold the potential to catalyze advancements in manufacturing processes within the realm of advanced materials, thereby contributing to

broader efforts aimed at enhancing industrial efficiency, sustainability, and innovation.

ACKNOWLEDGMENTS

This work was supported by the Scientific and Technological Research Council of Türkiye through the Scientific and Technological Research Projects Funding Program (TUBITAK 1001-221M085). The authors gratefully thank Professor Kenan Danisman for his invaluable guidance, support, and feedback during the coating of titanium nitride layers.

DATA AVAILABILITY STATEMENT

The data that support the findings of this study are available from the corresponding author upon reasonable request.

ORCID

Ahmed Cagri Sayin https://orcid.org/0009-0008-8666-7995
Sengul Danisman https://orcid.org/0000-0002-2720-5685
Emin Ersoy https://orcid.org/0000-0002-6260-8084
Cagatay Yilmaz https://orcid.org/0000-0002-8063-151X
Sinan Kesriklioglu https://orcid.org/0000-0002-2914-808X

REFERENCES

1. Matykiewicz D. Hybrid epoxy composites with both powder and fiber filler: a review of mechanical and thermomechanical properties. *Materials*. 2020;13:1802. doi:10.3390/MA13081802
2. Khedri E, Karimi HR, Mohamadi R, Aliha MRM, Masoudi NR. Mechanical, fracture, and environmental performance of greener polymer composites containing low to high micro fillers with recycled and byproduct origins. *Polym Compos*. 2024;45:8694-8709. doi:10.1002/PC.28369
3. Koklu U, Morkavuk S, Featherston C, et al. The effect of cryogenic machining of S2 glass fibre composite on the hole form and dimensional tolerances. *Int J Adv Manuf Technol*. 2021;115(1):125-140. doi:10.1007/s00170-021-07150-y
4. Jasper S, Ravichandran M, Vijayakumar D. Experimental investigation on end milling of GFRP by using Taguchi optimization. *Mater Today Proc*. 2023;72:2261-2267. doi:10.1016/j.matpr.2022.09.214
5. Homrighausen CL, Mereness AS, Schutte EJ, Williams B, Young NE, Blackburn R. Fabrication, evaluation and radiation behavior of S2-glass fiber reinforced polyimide laminates for cryogenic applications. *High Perform Polym*. 2007;19:382-400. doi:10.1177/0954008307077769
6. Dhand V, Mittal G, Rhee KY, Park SJ, Hui D. A short review on basalt fiber reinforced polymer composites. *Compos B Eng*. 2015;73:166-180. doi:10.1016/j.compositesb.2014.12.011
7. Doğru MH, Yeter E, Göv İ, Göv K. Ballistic impact resistance and flexural performance of natural basalt fiber with carbon and glass fibers in inter-ply hybrid composites. *Polym Compos*. 2024;45:9785-9801. doi:10.1002/PC.28438
8. Deák T, Czigány T. Chemical composition and mechanical properties of basalt and glass fibers: a comparison. *Text Res J*. 2009;79:645-651. doi:10.1177/0040517508095597
9. Song J, Liu J, Zhang H, et al. PVDF/PMMA/basalt fiber composites: morphology, melting and crystallization, structure, mechanical properties, and heat resistance. *J Appl Polym Sci*. 2014;131:40494. doi:10.1002/app.40494
10. Chegdani F, Mezghani S, El Mansori M, Mkaddem A. Fiber type effect on tribological behavior when cutting natural fiber reinforced plastics. *Wear*. 2015;332-333:772-779. doi:10.1016/j.wear.2014.12.039
11. Davim JP, Reis P. Damage and dimensional precision on milling carbon fiber-reinforced plastics using design experiments. *J Mater Process Technol*. 2005;160:160-167. doi:10.1016/j.jmatprotec.2004.06.003
12. Li ZC, Jiao Y, Deines TW, Pei ZJ, Treadwell C. Rotary ultrasonic machining of ceramic matrix composites: feasibility study and designed experiments. *Int J Mach Tools Manuf*. 2005;45:1402-1411. doi:10.1016/j.ijmachtools.2005.01.034
13. Sun H, Xiang D, Liu Z, et al. Failure analysis of glass fiber and basalt fiber reinforced polymer composites under an extreme environment with high-temperature, high-pressure and H_2S/CO_2 exposure. *Polym Compos*. 2024;45:10124-10136. doi:10.1002/PC.28462
14. Varma M, Chandran S, Vijay Kumar V, Suyambulingam I, Siengchin S. A comprehensive review on the machining and joining characteristics of natural fiber-reinforced polymeric composites. *Polym Compos*. 2024;45(6):4850-4875. doi:10.1002/PC.28148
15. Colligan K, Ramulu M, Colligan K, Ramulu M. Delamination in surface plies of graphite/epoxy caused by the edge trimming process. *pmcm*. 1991;112:113-125. Accessed April 17, 2024. https://ui.adsabs.harvard.edu/abs/1991pmcm.proc..113C/abstract
16. Gao T, Zhang Y, Li C, et al. Fiber-reinforced composites in milling and grinding: machining bottlenecks and advanced strategies. *Front Mech Eng*. 2022;17:24. doi:10.1007/s11465-022-0680-8
17. Sarma PMMS, Karunamoorthy L, Palanikumar K. Modeling and analysis of cutting force in turning of GFRP composites by CBN tools. *J Reinf Plast Compos*. 2008;27:711-723. doi:10.1177/0731684407084214
18. Hocheng H, Tsao CC. Effects of special drill bits on drilling-induced delamination of composite materials. *Int J Mach Tools Manuf*. 2006;46:1403-1416. doi:10.1016/j.ijmachtools.2005.10.004
19. Jenarthanan MP, Prakash AL, Jeyapaul R. Mathematical modeling of delamination factor on end milling of hybrid GFRP composites through RSM. *Pigment Resin Technol*. 2016;45:371-379. doi:10.1108/PRT-08-2015-0083
20. Kilickap E. Analysis and modeling of delamination factor in drilling glass fiber reinforced plastic using response surface methodology. *J Compos Mater*. 2011;45:727-736. doi:10.1177/0021998310381539
21. Stone R, Krishnamurthy K. A neural network thrust force controller to minimize delamination during drilling of graphite-epoxy laminates. *Int J Mach Tools Manuf*. 1996;36:985-1003. doi:10.1016/0890-6955(96)00013-2
22. Colligan K, Ramulu M. The effect of edge trimming on composite surface plies. *Am Soc Mech Eng Manuf Rev*. 1992;5(4):274-283.

23. Chockalingam P, Kuang KC, Vijayaram TR. Effects of grinding process parameters and coolants on the grindability of GFRP laminates. *Mater Manuf Process*. 2013;28:1071-1076. doi:10.1080/10426914.2013.792411
24. Jenarthanan MP, Jeyapaul R. Optimisation of machining parameters on milling of GFRP composites by desirability function analysis using Taguchi method. *Int J Eng Sci Technol*. 2018;5:22-36. doi:10.4314/ijest.v5i4.3
25. Nayak D, Bhatnagar N, Mahajan P. Machining studies of unidirectional glass fiber reinforced plastic (UD-GFRP) composites part 1: effect of geometrical and process parameters. *Mach Sci Technol*. 2005;9:481-501. doi:10.1080/10910340500398167
26. Masek P, Zeman P, Kolar P, Holesovsky F. Edge trimming of C/PPS plates. *Int J Adv Manuf Technol*. 2019;101:157-170. doi:10.1007/s00170-018-2857-1
27. Ceritbinmez F, Yapici A, Kanca E. The effect of nanoparticle additive on surface milling in glass fiber reinforced composite structures. *Polym Polym Compos*. 2021;29:S575-S585. doi:10.1177/09673911211014172
28. Ekici E, Motorcu AR, Polat A. Optimization and alternative image processing approach for the comprehensive assessment of delamination and uncut fiber in drilling fiber metal laminate. *J Braz Soc Mech Sci Eng*. 2022;44:502. doi:10.1007/s40430-022-03806-2
29. Venkateshwaran N, ElayaPerumal A. Hole quality evaluation of natural fiber composite using image analysis technique. *J Reinf Plast Compos*. 2013;32:1188-1197. doi:10.1177/0731684413486847
30. Hrechuk A, Bushlya V, Ståhl JE. Hole-quality evaluation in drilling fiber-reinforced composites. *Compos Struct*. 2018;204:378-387. doi:10.1016/j.compstruct.2018.07.105
31. Isaev A, Grechishnikov V, Pivkin P, Mihail K, Ilyuhin Y, Vorotnikov A. Machining of thin-walled parts produced by additive manufacturing technologies. *Proc CIRP*. 2016;41:1023-1026. doi:10.1016/j.procir.2015.08.088
32. Venu Gopala Rao G, Mahajan P, Bhatnagar N. Machining of UD-GFRP composites chip formation mechanism. *Compos Sci Technol*. 2007;67(11–12):2271-2281. doi:10.1016/j.compscitech.2007.01.025
33. Azmi AI, Lin RJT, Bhattacharyya D. Experimental study of machinability of GFRP composites by end milling. *Mater Manuf Process*. 2012;27:1045-1050. doi:10.1080/10426914.2012.677917
34. Yardimeden A. Investigation of optimum cutting parameters and tool radius in turning glass-fiber-reinforced composite material. *Sci Eng Compos Mater*. 2016;23:85-92. doi:10.1515/secm-2013-0301
35. Naveen Sait A, Aravindan S, Noorul HA. Optimisation of machining parameters of glass-fibre-reinforced plastic (GFRP) pipes by desirability function analysis using Taguchi technique. *Int J Adv Manuf Technol*. 2009;43:581-589. doi:10.1007/s00170-008-1731-y
36. Bobzin K. High-performance coatings for cutting tools. *CIRP J Manuf Sci Technol*. 2017;18:1-9. doi:10.1016/j.cirpj.2016.11.004
37. Velraja K, Srinivasan V. Analysis of DC magnetron sputtered coatings for life time improvement (LTI). *Mater Today Proc*. 2022;66:845-849. doi:10.1016/j.matpr.2022.04.454
38. Subhedar DG, Chauhan KV, Patel DA. An experimental investigation of TiN coating on cutting force and surface finish in milling of aluminium. *Mater Today Proc*. 2022;59:161-165. doi:10.1016/j.matpr.2021.10.384
39. Knap A, Dvořáčková Š, Knápek T. Study of the machining process of GFRP materials by milling technology with coated tools. *Coatings*. 2022;12:1354. doi:10.3390/coatings12091354
40. Köpf A, Feistritzer S, Udier K. Diamond coated cutting tools for machining of non-ferrous metals and fibre reinforced polymers. *Int J Refract Met Hard Mater*. 2006;24:354-359. doi:10.1016/j.ijrmhm.2005.11.013
41. Kelly PJ, Hisek J, Zhou Y, Pilkington RD, Arnell RD. Advanced coatings through pulsed magnetron sputtering. *Surf Eng*. 2004;20:157-162. doi:10.1179/026708404225010702
42. Haubner R, Lessiak M, Pitonak R, Köpf A, Weissenbacher R. Evolution of conventional hard coatings for its use on cutting tools. *Int J Refract Met Hard Mater*. 2017;62:210-218. doi:10.1016/j.ijrmhm.2016.05.009
43. Atta S, NarendraKumar U, Kumar KVANPS, Yadav DP, Dash S. Recent developments and applications of TiN-based films synthesized by magnetron sputtering. *J Mater Eng Perform*. 2023;32:9979-10015. doi:10.1007/s11665-023-08273-x
44. Ait Djafer AZ, Saoula N, Madaoui N, Zerizer A. Deposition and characterization of titanium carbide thin films by magnetron sputtering using Ti and TiC targets. *Appl Surf Sci*. 2014;312:57-62. doi:10.1016/j.apsusc.2014.05.084
45. Mkaddem A, Ben Soussia A, El Mansori M. Wear resistance of CVD and PVD multilayer coatings when dry cutting fiber reinforced polymers (FRP). *Wear*. 2013;302:946-954. doi:10.1016/j.wear.2013.03.017
46. Çalişkan H, Kurbanoğlu C, Panjan P, Čekada M, Kramar D. Wear behavior and cutting performance of nanostructured hard coatings on cemented carbide cutting tools in hard milling. *Tribol Int*. 2013;62:215-222. doi:10.1016/j.triboint.2013.02.035
47. Paulitsch J, Schenkel M, Zufraß T, Mayrhofer PH, Münz WD. Structure and properties of high power impulse magnetron sputtering and DC magnetron sputtering CrN and TiN films deposited in an industrial scale unit. *Thin Solid Films*. 2010;518:5558-5564. doi:10.1016/j.tsf.2010.05.062
48. Boehlerit: Startseite. Schneidwalze—Vom Rohling zum einsatzfertigen Schneidsystem. Accessed April 17, 2024. https://www.boehlerit.com/
49. Chun SY. A comparative study of superhard TiN coatings deposited by DC and inductively coupled plasma magnetron sputtering. *J Korean Inst Surf Eng*. 2013;46:55-60. doi:10.5695/jkise.2013.46.2.055
50. Schneider CA, Rasband WS, Eliceiri KW. NIH image to ImageJ: 25 years of image analysis. *Nat Methods*. 2012;9:671-675. doi:10.1038/nmeth.2089
51. Danışman Ş, Odabaş D, Teber M. The effect of TiN, TiAlN, TiCN thin films obtained by reactive magnetron sputtering method on the wear behavior of Ti_6Al_4V alloy: a comparative study. *Coatings*. 2022;12:1238. doi:10.3390/coatings12091238
52. Xian G, Xiong J, Fan H, et al. Investigations on microstructure, mechanical and tribological properties of TiN coatings deposited on three different tool materials. *Int J Refract Met Hard Mater*. 2022;102:105700. doi:10.1016/j.ijrmhm.2021.105700
53. Jones MI, McColl IR, Grant DM. Effect of substrate preparation and deposition conditions on the preferred orientation

of TiN coatings deposited by RF reactive sputtering. *Surf Coatings Technol*. 2000;132:143-151. doi:10.1016/S0257-8972(00)00867-7

54. Chen T, Gao F, Li S, Liu X. The comparative study on cutting performance of different-structure milling cutters in machining CFRP. *Appl Sci*. 2018;8:1353. doi:10.3390/app8081353
55. Bayraktar S, Turgut Y. Investigation of the cutting forces and surface roughness in milling carbon-fiber-reinforced polymer composite material. *Mater Tehnol*. 2016;50:591-600. doi:10.17222/mit.2015.199
56. Ashmawi TH, Lebrão GW, Lebrão SMG, Bordinassi ÉC. Study of surface roughness and burr formation after milling of carbon fiber/titanium stacks. *Mater Res*. 2020;22. doi:10.1590/1980-5373-MR-2019-0388
57. Savaş S, Danişman Ş. Multipass sliding wear behavior of TiAlN coatings using a spherical indenter: effect of coating parameters and duplex treatment. *Tribol Trans*. 2014;57:242-255. doi:10.1080/10402004.2013.868564
58. Pei YT, Chen CQ, Shaha KP, et al. Microstructural control of TiC/a-C nanocomposite coatings with pulsed magnetron sputtering. *Acta Mater*. 2008;56:696-709. doi:10.1016/j.actamat.2007.10.025
59. Hosokawa A, Hirose N, Ueda T, Furumoto T. High-quality machining of CFRP with high helix end mill. *CIRP Ann*. 2014;63:89-92. doi:10.1016/j.cirp.2014.03.084
60. Praveen Raj P, Pazhanivel K, Elaya PA. Taguchi analysis of tool wear and delamination in milling of GFRP composite using coated K10 end mill. *Prog Ind Ecol*. 2018;12:138. doi:10.1504/PIE.2018.095883
61. Ozkan D, Panjan P, Gok MS, Karaoglanli AC. Investigation of machining parameters that affects surface roughness and cutting forces in milling of CFRPs with TiAlN and TiN coated carbide cutting tools. *Mater Res Express*. 2019;6:095616. doi:10.1088/2053-1591/ab30de
62. Ben SA, Mkaddem A, El Mansori M. Effect of coating type on dry cutting of glass/epoxy composite. *Surf Coatings Technol*. 2013;215:413-420. doi:10.1016/j.surfcoat.2012.04.098
63. Murphy C, Byrne G, Gilchrist MD. The performance of coated tungsten carbide drills when machining carbon fibre-reinforced epoxy composite materials. *Proc Inst Mech Eng Part B J Eng Manuf*. 2002;216:143-152. doi:10.1243/0954405021519735
64. Benyettou R, Amroune S, Slamani M, et al. Assessment of induced delamination drilling of natural fiber reinforced composites: a statistical analysis. *J Mater Res Technol*. 2022;21:131-152. doi:10.1016/j.jmrt.2022.08.161
65. Wang H, Sun J, Li J, Li W. Roughness modelling analysis for milling of carbon fibre reinforced polymer composites. *Mater Technol*. 2015;30:A46-A50. doi:10.1179/1753555715Y.0000000002

How to cite this article: Sayin AC, Danisman S, Ersoy E, Yilmaz C, Kesriklioglu S. Experimental and statistical damage analysis in milling of S2-glass fiber/epoxy and basalt fiber/epoxy composites. *Polym Compos*. 2024;45(16):15140-15158. doi:10.1002/pc.28826